

# Spin Hall magnetoresistance at the altermagnetic insulator/Pt interface

Miina Leiviskä<sup>a,\*</sup>,<sup>1</sup> Reza Firouzmandi<sup>a</sup>,<sup>2</sup> Kyo-Hoon Ahn,<sup>1</sup> Peter Kubaščík,<sup>3</sup> Zbynek Soban,<sup>1</sup> Satya Prakash Bommanaboyena,<sup>1</sup> Christoph Müller,<sup>1</sup> Dominik Kriegner,<sup>1</sup> Sebastian Sailler,<sup>4</sup> Michaela Lammel,<sup>4</sup> Kranthi Kumar Bestha,<sup>2,5</sup> Libor Šmejkal,<sup>6,7,1</sup> Jakub Zelezny,<sup>1</sup> Anja U. B. Wolter,<sup>2</sup> Monika Scheufele,<sup>8,9</sup> Johanna Fischer,<sup>10</sup> Matthias Opel,<sup>8</sup> Stephan Geprägs,<sup>8</sup> Matthias Althammer,<sup>8</sup> Bernd Büchner,<sup>2,11,12</sup> Tomas Jungwirth,<sup>1,13</sup> Lukáš Nádvořník,<sup>3</sup> Sebastian T. B. Goennenwein,<sup>4</sup> Vilmos Kocsis,<sup>2</sup> and Helena Reichlova<sup>1</sup>

<sup>1</sup>*Institute of Physics, Czech Academy of Sciences, Prague, Czechia*

<sup>2</sup>*Institut für Festkörperforschung, Leibniz IFW Dresden, 01069 Dresden, Germany*

<sup>3</sup>*Faculty of Mathematics and Physics, Charles University, Prague, Czechia*

<sup>4</sup>*Department of Physics, University of Konstanz, Konstanz, Germany*

<sup>5</sup>*Institute of Solid State and Materials Physics, TU Dresden, Dresden, Germany*

<sup>6</sup>*Max Planck Institute for the Physics of Complex Systems, Dresden, Germany*

<sup>7</sup>*Max Planck Institute for Chemical Physics of Solids, Dresden, Germany*

<sup>8</sup>*Walther-Meißner-Institut, Bayerische Akademie der Wissenschaften, Garching, Germany*

<sup>9</sup>*Technical University of Munich, TUM School of Natural Sciences, Physics Department, Garching, Germany*

<sup>10</sup>*Université Grenoble Alpes, CEA, CNRS, Spintec, Grenoble, France*

<sup>11</sup>*Institute of Solid State and Materials Physics and Würzburg-Dresden Cluster of Excellence ct.qmat, Technische Universität Dresden, 01062 Dresden, Germany*

<sup>12</sup>*Center for Transport and Devices, Technische Universität Dresden, 01069 Dresden, Germany*

<sup>13</sup>*School of Physics and Astronomy, University of Nottingham, Nottingham, UK*

The resistance of a heavy metal can be modulated by an adjacent magnetic material through the combined effects of the spin Hall effect, inverse spin Hall effect, and dissipation of the spin accumulation at the interface. This phenomenon is known as spin Hall magnetoresistance. The dissipation of the spin accumulation can occur via various mechanisms, with spin-transfer torque being the most extensively studied. In this work, we report the observation of spin Hall magnetoresistance at the interface between platinum and an insulating altermagnetic candidate, Ba<sub>2</sub>CoGe<sub>2</sub>O<sub>7</sub>. Our findings reveal that this heterostructure exhibits a relatively large spin Hall magnetoresistance signal, which is anisotropic with respect to the crystal orientation of the current channel. We explore and rule out several potential explanations for this anisotropy and propose that our results may be understood in the context of the anisotropic altermagnetic ordering of Ba<sub>2</sub>CoGe<sub>2</sub>O<sub>7</sub>.

## I. INTRODUCTION

Spin Hall magnetoresistance (SMR) is an actively researched magnetoresistive effect present in bilayers of a magnet - here insulating (MI) - and a heavy metal (HM) [1–3]. It relies on the concerted action of spin Hall (SHE) and inverse spin Hall effects (ISHE): driving a current ( $\mathbf{j}_c$ ) in the HM layer generates a spin accumulation ( $\boldsymbol{\mu}_s$ ) at the HM|MI interface via SHE and depending on the spin transparency of this interface the generated spin current ( $\mathbf{j}_s$ ) can flow into the MI ( $\mathbf{j}_s^{\text{abs}}$ ) while any back-reflected spin current ( $\mathbf{j}_s^{\text{ref}}$ ) is re-converted to a charge current via ISHE. This process is illustrated in Figure 1a. The spin current transparency of the interface is sensitive to the (sublattice) magnetic moment direction ( $\mathbf{m}$ ) of the MI layer - rotating  $\mathbf{m}$  will modulate the resistivity of the HM layer. Typically, when  $\boldsymbol{\mu}_s$  and  $\mathbf{m}$  are parallel more spin current is reflected back at the HM|MI interface resulting in a low-resistance state, while when  $\boldsymbol{\mu}_s$  and  $\mathbf{m}$  are perpendicular to each other, more spin current is absorbed by the MI resulting in a high-resistance state. The SMR ratio, which quantifies the relative resistance difference between these two states, is typically of the order of 0.01% in MI/Pt heterostructures [3–10].

In the initial theoretical models describing the SMR, the variation of the interface spin-current transparency as a function of the relative angle of  $\boldsymbol{\mu}_s$  and  $\mathbf{m}$  was explained in terms of the spin-transfer torque (STT) at the interface [2]: if  $\boldsymbol{\mu}_s$  and  $\mathbf{m}$  are parallel, STT is zero and the spin current is reflected back while if  $\boldsymbol{\mu}_s$  and  $\mathbf{m}$  are perpendicular, maximum STT is exerted on  $\mathbf{m}$  and the spin current is absorbed by the MI. However, in principle any mechanism through which the spin accumulation can dissipate from the interface will contribute to the SMR ratio. For example, thermal fluctuations allow for spin-flip scattering at the interface and give rise to injection/annihilation of thermal magnons, resulting in a maximum flow of spin current when  $\mathbf{m} \parallel \boldsymbol{\mu}_s$  [11–15]. A recent theoretical work by Reiss *et al.* provides a comprehensive account of the various channels through which spin current can enter the MI layer [16]. In dc-measurements on HM|MI heterostructures, three primary contributions (summarized in Figure 1b) are expected: i) STT and spin-pumping at the HM|MI interface, ii) incoherent thermal magnon creation/annihilation at the HM|MI interface, and iii) magnon capacitance (i.e. accumulation and dissipation of magnons in the MI).

Altermagnets are a newly identified class of collinear compensated magnets which differ from antiferromagnets by their combined spin and crystal symmetry. Altermagnets have characteristic spin-degenerate nodes and alternating even-parity spin polarization splitting that breaks time-reversal symmetry [17–20]. They exhibit unconventional properties

<sup>a</sup> These authors contributed equally. \*leiviska@fzu.cz

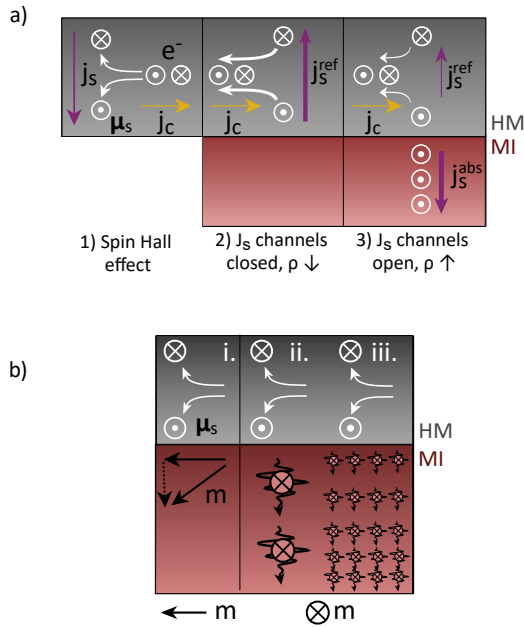


FIG. 1. (Color Online) a) Spin Hall magnetoresistance in HM/MI heterostructures, where charge current ( $j_c$ ) generates a spin current (1) that can be either reflected ( $j_s^{\text{ref}}$ ) or absorbed ( $j_s^{\text{abs}}$ ) at the interface depending on the available spin current channels across the interface (2,3). When there are no available channels the spin current is reflected and converted back to charge current (2) and when the channels are open the spin current is absorbed by the MI (3). This modulates the resistivity of the HM. b) Three channels contributing to the SMR ratio in magnetic insulators in the DC-limit: i. STT and spin pumping, ii. excitation of longitudinal magnons, and iii. magnon capacitance. Channel i. is relevant when  $\mu_s \perp m$  and channels ii. and iii. are relevant when  $\mu_s \parallel m$ .

that are potentially favorable for spintronics and magnonics, such as the unconventional anomalous Hall effect [21, 22], the generation of highly anisotropic and strongly spin-polarized currents in the absence of a net magnetization [23–26], the accompanying unconventional giant/tunneling magnetoresistance [27, 28] and spin-torque effects [25, 26], or anisotropic chirality-split magnon dispersions in the absence of external magnetic field [29, 30]. Notably, also the record SMR ratio (0.25 %) has been observed in heterostructures of Pt and the insulating altermagnetic candidate  $\alpha$ -Fe<sub>2</sub>O<sub>3</sub> [10]. This greatly surpasses the SMR ratio in heterostructures incorporating ferromagnetic insulators, such as yttrium ion garnet (0.16 %) [3], and antiferromagnetic insulators, such as NiO (0.08 %) [9]. This may suggest that the type of magnetic ordering of the MI plays a role in determining the SMR ratio.

In this work, we present our measurements of SMR in an altermagnetic and ferroelectric insulator Ba<sub>2</sub>CoGe<sub>2</sub>O<sub>7</sub> (BCGO) [31]. We first detail the fabrication of devices for SMR experiments on bulk single crystals of BCGO, followed by the analysis of the SMR features on BCGO/Pt heterostructures. Notably, we show that the SMR ratio (of the order of  $2 \times 10^{-4}$ ) is anisotropic depending on the crystal direction of the applied current. We discuss this observation in the context of

various factors such as magnetic domains, magnetocrystalline anisotropy, electric polarization, and the crystal symmetries characterizing the altermagnetic phase. Finally, we suggest mechanisms including anisotropic spin mixing conductance and anisotropic magnon dispersion through which the altermagnetic phase of BCGO could give rise to the observed anisotropy.

## II. SMR IN Ba<sub>2</sub>CoGe<sub>2</sub>O<sub>7</sub>/Pt HETEROSTRUCTURES

Ba<sub>2</sub>CoGe<sub>2</sub>O<sub>7</sub> (BCGO) is an insulating altermagnet that crystallizes in a non-centrosymmetric tetragonal structure in space group  $P4_21m$  (Figure 2a) [32, 33] and belongs to the spin-point group  $14_2m^2m$  [31]. Below the critical temperature of 6.7 K, the sublattice magnetic moments residing on the Co<sup>2+</sup> ions adopt an antiparallel configuration in the (001) plane [33]. A finite DMI-vector along the [001] direction allows for the slight in-plane canting of the sublattice moments and thus a weak magnetization, the extent of which depends on the orientation of the sublattice moments but is of the order of  $0.01 \mu_B/\text{f.u.}$  [34–37]. BCGO is also ferroelectric below the critical temperature of 6.7 K - the finite polarization has been attributed to the p-d hybridization between the transition metal and the ligand [36, 38]. Upon the in-plane rotation of the sublattice magnetic moments,  $P_x$  and  $P_y$  are zero while  $P_z$  shows cosine dependency with maximum  $P_z$  when the magnetic field is parallel to  $\langle 110 \rangle$  [36, 38]. When a strong out-of-plane field (order of 5 T) is applied, the spins cant away from the (001)-plane, which results in the  $P_z$  decreasing and  $P_x$  and  $P_y$  becoming finite [36, 38].

The single crystal of BCGO was grown by the floating zone method in the presence of artificial air (80 % N<sub>2</sub> and 20 % O<sub>2</sub>). The [001] normal surfaces were polished using Al<sub>2</sub>O<sub>3</sub> lapping films (261X, 3M) up to 0.3  $\mu\text{m}$  surface quality. The final surface quality of  $\sim 5$  nm was realized with chemical-mechanical polishing using 0.02  $\mu\text{m}$  silica suspension (MasterMet2, Buehler). X-ray diffraction measurements, shown in Figure 2b-d, were carried out to confirm the crystallographic structure and orientation of our BCGO bulk sample with a Rigaku Smartlab diffractometer in the parallel beam configuration (using Cu-K $\alpha_1$  radiation). A pole figure was measured for the {201} planes to confirm the single-crystalline nature and the four-fold rotational symmetry of the tetragonal crystal structure as shown in Figure 2b. Four {201} poles (or diffraction maxima) are observed with an azimuthal periodicity of 90° as expected. The relevant in-plane crystallographic directions were determined based on the azimuthal dependence. A symmetric radial scan ( $2\theta/\omega$ ) measured with this alignment is presented in Figure 2c. Using these peak positions and a reciprocal space map, lattice constants of  $a = b = 8.39 \text{ \AA}$ ,  $c = 5.55 \text{ \AA}$  are extracted, which are in excellent agreement with the values reported earlier for BCGO [32]. Both the pole figure and the rocking curve of the (002) Bragg reflection (see Figure 2d) demonstrate that the (001) lattice planes are parallel to the sample surface. We have also measured the chemical composition of the bulk crystals using X-ray fluorescence and the obtained stoichiometry of Ba<sub>2.03</sub>Co<sub>1.01</sub>Ge<sub>1.96</sub>O<sub>7</sub> is very close

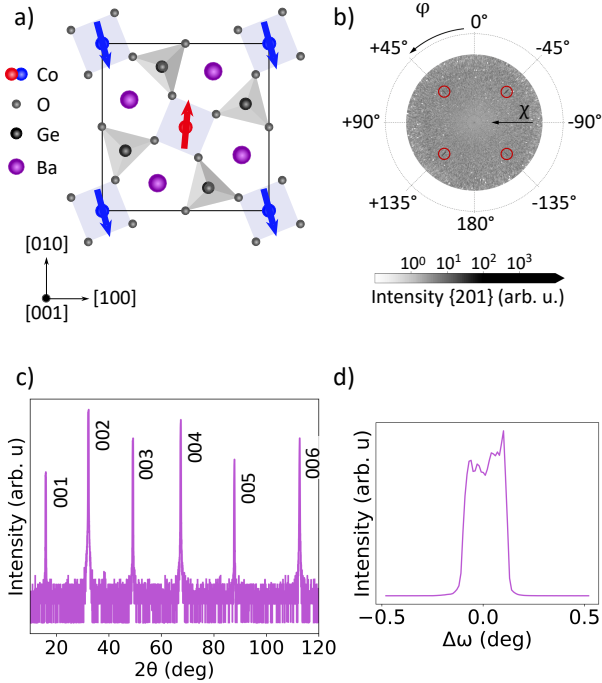


FIG. 2. (Color Online) a) The crystal structure of BCGO. The spins of the magnetic sublattices are marked in red and blue and the spin canting is exaggerated for the sake of clarity. b-d) Structural characterization of the BCGO single crystal at 300 K: b) the  $\{201\}$  pole figure, c) a radial scan (the intensity is plotted on logarithmic scale), and d) a rocking curve around (002). Note that the shape of the rocking curve is not a consequence of detector saturation.

to the nominal one of  $\text{Ba}_2\text{CoGe}_2\text{O}_7$ .

We have confirmed the very small magnetization in our samples by SQUID magnetometry as shown in Figure 3a-c, compatible with a compensated magnetic order with slightly canted moments in-plane. The magnetization as a function of temperature, field, and field orientation was measured using the horizontal rotator option (MPMS3, Quantum Design). First, in Figure 3a, we have identified the critical temperature as  $\sim 7$  K, which is in good agreement with the previously reported value of 6.7 K [34, 35]. As shown in Figure 3b, we observe a small spontaneous net moment of  $\sim 0.01 \mu_B/\text{f.u.}$  along the [100] and [110] directions, and vanishing spontaneous moment in the [001] direction, which is in agreement with the easy-plane anisotropy as well as DMI-allowed moment canting in the (001) plane [34, 36, 37]. Considering the slightly larger magnetization when  $H \parallel [100]$  (sublattice magnetic moments perpendicular to  $H$ ) seen in field-sweeps and the in-plane field orientation scans shown in Figure 3b and c, respectively, we also identify  $\langle 100 \rangle$  as the slightly easier axes of the sublattice moments. Note that as shown in Figure 3c this anisotropy is not present at 1.9 T, which is the field used for the SMR measurements later on.

Moreover, we have confirmed the ferroelectric nature of our sample by measuring the polarization along [001], as shown in Figure 3d. The ferroelectric polarization was measured on a

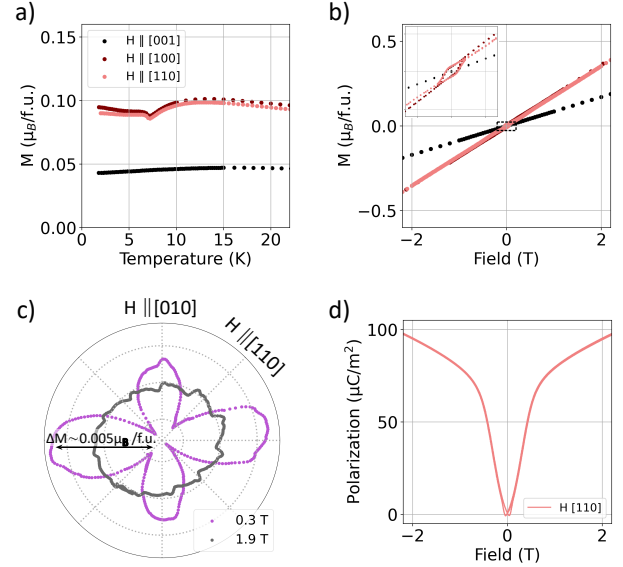


FIG. 3. (Color Online) a) Temperature-dependence of the magnetization along the external magnetic field measured under a 0.5 T field along different crystal axes. b) Field-dependence of the magnetization measured at 2 K with the field along different crystal axes. The inset is a close-up of the plot marked with the dashed rectangle (in the range 0.2 to  $-0.2$  T and  $0.05$  to  $-0.05 \mu_B/\text{f.u.}$ ). See a) for the legend. c) The change in magnetization plotted as  $\frac{M - \langle M \rangle}{\langle M \rangle}$ , where  $\langle M \rangle$  is the average magnetization, as a function of the in-plane field orientation at 2 K. d) The magnetic field-dependence of the polarization along the [001]-direction at 2.5 K when the field is applied along the [110]-direction.

thin slab of sample using an electrometer in charge measurement mode (6517A, Keithley) and a cryostat (PPMS, Quantum Design). A finite polarization along the [001] axis is observed when the spins align along the oxygen-oxygen bonds of the  $\text{CoO}_4$  tetrahedra - upon 90 degree rotation this polarization reverses the sign whereas upon 45 degree rotation it vanishes [38]. Applying a magnetic field along the [110] axis will align the spins along the oxygen-oxygen bond and thus yield a finite polarization along the [001] axis, as we see in Figure 3d. This is in good agreement with previous reports [38]. Removing the magnetic field returns the system to a multidomain state where an equal population of the four magnetic domains with mutually orthogonal Néel vector orientations [39] will result in the vanishing polarization.

For the SMR measurements, Hall bar structures (width =  $50 \mu\text{m}$ , length =  $600 \mu\text{m}$ ) with different orientations of the current direction with respect to the BCGO  $[1\bar{1}0]$  crystal axis (defined by angle  $\alpha$ ) were patterned on the polished BCGO (001) surface with e-beam lithography followed by a deposition of 15 nm of Pt through sputtering (Pt resistivity is of the order of  $80 \mu\Omega\text{cm}$ ). After this, the contact pads were pat-

terned by depositing Ti(5)/Au(80 nm) and a subsequent lift-off process. The final devices are shown in the inset of Figure 4a. To measure the SMR signal, we rotated an external field of 1.9 T in three mutually perpendicular planes - in-plane (ip), out-of-plane perpendicular to the current  $j$  (oopj), and out-of-plane parallel to  $j$ , (oopt) - while measuring the longitudinal Pt resistivity ( $\rho_{xx}$ ) at a temperature of 2 K. At 2 K we are well below the critical magnetic ordering temperature, and at 1.9 T well above the in-plane monodomainization field and the in-plane magnetocrystalline anisotropy field [33, 40] so we assume a smooth rotation of the magnetic order parameter in-plane.

We first focus on the results obtained for a Hall bar with the current direction aligned with the BCGO [100]-direction ( $\alpha = 45$  deg). The modulation of  $\rho_{xx}$  during the three field rotations is shown in Figure 4a (plotted as  $\rho_{xx}/\rho_{xx,0} - 1$ , where  $\rho_{xx,0}$  is the Pt resistivity when the magnetic field is parallel to the current, i.e.  $\phi = 0$ ). In the in-plane scans we observe a typical SMR response of a  $-\cos 2\phi$ , where  $\phi$  is the angle between the magnetic field and the current. This behavior is the same as in other systems where the sublattice moments align perpendicular to the magnetic field [5, 8–10], indicating that the signal is governed by the sublattice moment orientation rather than that of the weak net magnetization. The temperature-dependence of the SMR signal shown in Figure 4b matches well with temperature dependent magnetic ordering of BCGO as shown in Figure 3a. The positive SMR signal vanishes above the critical temperature indicating that the signal is related to the magnetic order of BCGO. The small negative SMR signal ( $\sim -1 \times 10^{-5}$ ) right above the critical temperature may originate from the paramagnetic moments aligning with the external field [41–43].

In the two out-of-plane scans we observe behavior similar to that in  $\alpha$ -Fe<sub>2</sub>O<sub>3</sub> [10]: in the oopj (oopt) planes the SMR exhibits plateaus at maximum (minimum) SMR, respectively, with deep dips (peaks). This indicates that the system likely breaks into a multidomain state when the field is out-of-plane (dips/peaks) while with an increasing in-plane component of the field the system transitions towards a monodomain state (plateaus). BCGO has two mutually orthogonal pairs of 180 deg magnetic domains that are degenerate when the field is along [001] direction [39], which supports the multidomain origin of the dips/peaks. However, compared to  $\alpha$ -Fe<sub>2</sub>O<sub>3</sub> [10], the plateaus are narrower and the peaks/dips are wider, which can be a result of different domain dynamics and magnetocrystalline anisotropies.

We note that the SMR ratio of  $\sim 2.5 \times 10^{-4}$  is surprisingly large considering that the Pt has been deposited *ex situ* without any treatment of the interface to remove possible impurities, the Pt thickness here is much larger than the spin diffusion length of Pt, and the temperature is very low. The SMR ratio is already comparable to heterostructures with Pt interfaced with conventional antiferromagnets such as NiO with *ex situ* grown Pt and optimized Pt thickness [8]. Optimizing the interface quality and the Pt thickness can further increase the SMR ratio [6, 44–47], highlighting the question whether alternating ferromagnetic insulators show higher SMR ratio compared to their ferromagnetic and antiferromagnetic insulator counterparts.

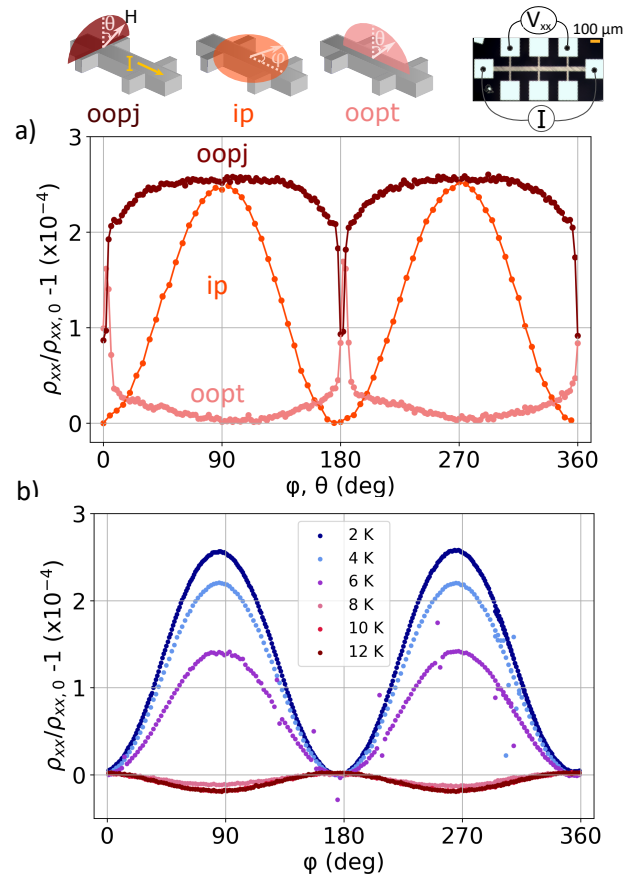


FIG. 4. (Color Online) a) The SMR signal in BCGO/Pt heterostructure at 2 K for  $\mathbf{j}_c \parallel [100]$ . A 1.9 T field is rotated in three perpendicular planes (ip, oopj, oopt). The top left inset shows the definitions of the field rotation planes and the top right inset is an optical image of the Hall bar devices. b) The temperature dependence of the SMR for ip-rotation of 1.9 T field. The positive SMR vanishes above the critical temperature of 6.7 K of BCGO.

Next, we measured the SMR ratio in Hall bars with different current orientations  $\alpha$ . In Figure 5, we show that the SMR ratio depends systematically on the direction of the current: when the current flows along  $[1\bar{1}0]$  or  $[110]$  ( $\alpha = 0$  or 90 deg, respectively), the SMR ratio is about a factor of two smaller than the SMR ratio when the current flows along  $[100]$  or  $[010]$  ( $\alpha = 45$  or 135 deg, respectively). This trend does not correlate with the Pt resistivity of each Hall bar at 2 K as confirmed in Figure 5b, indicating that the change in the SMR ratio is unlikely to stem purely from device-to-device variations. This is also corroborated by our observation of the same anisotropic behavior in separate, independently fabricated samples.

Next, to exclude different multidomain states as an explanation for the different SMR ratios between  $\alpha = 0$  and 90, and  $\alpha = 45$  and 135 deg devices, we have measured the field dependence of the SMR ratio. To that end, we have measured the field dependence of  $\rho_{xx}$  at  $\phi = 0$  and 90 deg: for  $\alpha = 0$  and 90 deg this means with the field along  $[1\bar{1}0]$  and  $[110]$ , and for  $\alpha = 45$  and 135 deg with the field along  $[100]$  and  $[010]$ . The



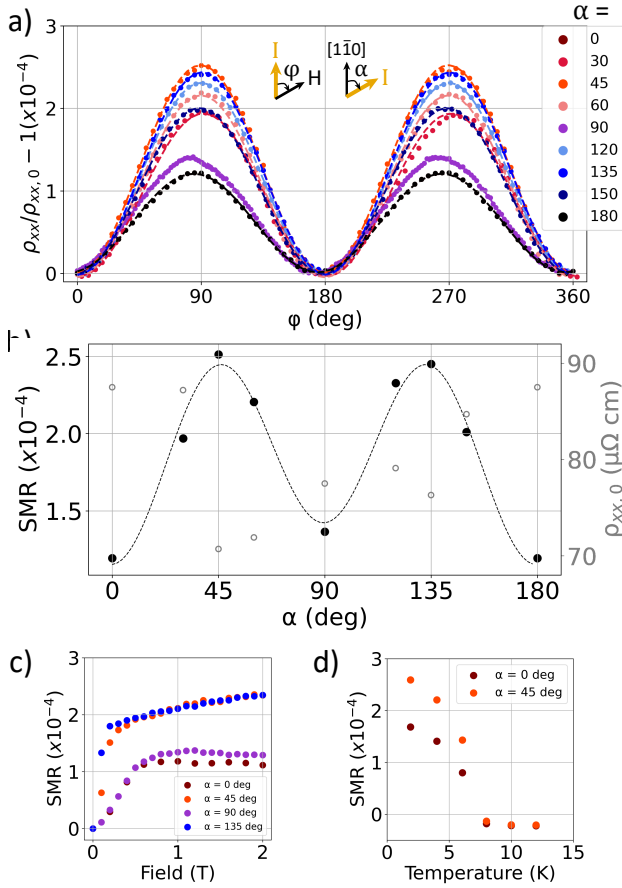


FIG. 5. (Color Online) a) The full ip angular scans of the SMR for different orientations of the current channel. The definitions for angles  $\varphi$  and  $\alpha$  are shown in the inset. The measurements were conducted at 2 K and under 1.9 T field. Note that the data for  $\alpha = 0$  and 180 deg is identical. b) The dependence of the SMR ratio (closed symbols) and the longitudinal resistivity (open symbols) at  $\varphi = 0$  deg on the current channel orientation  $\alpha$ . c) The field-dependence of the SMR ratio for  $\alpha = 0, 45, 90, 135$  deg. The slight amplitude variations compared to a) likely result from slight misalignment of the field orientation from perfectly parallel/perpendicular to the current channel. d) The temperature-dependence of the SMR ratio for  $\alpha = 0$  and 45 deg.

resulting field-dependence of the SMR ratio is plotted in Figure 5c. In the case of each  $\alpha$ , (relative) saturation is reached well below 1.9 T, suggesting a monodomain state in the in-plane field rotation measurements in Figure 5a. It should be noted, however, that the magnetocrystalline anisotropy observed in Figure 3c is also reflected in the slightly different saturation fields between  $\alpha = 0$  and 90 deg and  $\alpha = 45$  and 135 deg. Finally, the anisotropy disappears at 7 K along with the magnetic ordering of BCGO, as shown in Figure 5d.

We have also considered the possible influence of the electric polarization along the [001] axis ( $P_c$ ) on the SMR ratios. If we define angle  $\alpha'$  as the angle between the external magnetic field and the  $[1\bar{1}0]$  crystal axis, then  $P_c$  has roughly a  $-\cos 2\alpha'$  dependence, i.e.  $P_c$  is non-zero when the magnetic field is along  $\langle 100 \rangle$  direction and vanishes when the field is

along  $\langle 100 \rangle$  direction [38]. On the other hand, the angle  $\varphi$  in Figure 5a is defined as the angle between the current and the field so that for the different Hall bars, non-zero  $P_c$  is reached at different angles  $\varphi$ . If the non-zero  $P_c$  influenced the SMR amplitude we would expect to observe this influence at different  $\varphi$  for the different  $\alpha$ . In this case, we consider that observing a  $-\cos 2\varphi$  behavior for all  $\alpha$  would be unlikely and rather we would expect a more complex signal coming from the superposition of the  $-\cos 2\varphi$  (conventional SMR) and  $\cos 2\alpha'$  (influence of the  $P_c$ ) behaviors.

### III. DISCUSSION

As discussed above, we cannot explain the observed current orientation dependence of the SMR ratio in BCGO/Pt heterostructures via magnetocrystalline anisotropy, multidomain effects or polarization-induced changes as our SMR measurements are conducted under magnetic fields sufficient to saturate the SMR ratio and the symmetry of the variation in polarization is not compatible with that of the SMR ratio. We also note that the Hall bars measured here are all fabricated on the same surface. This ensures that - unlike in the case of anisotropic SMR observed in ferrimagnetic insulators [4, 48] - any sample-dependent variations in spin mixing conductance, such as differences in surface roughness or variations in magnetic ion area density for different crystal cuts should not contribute to the observed anisotropy. At the same time, if any of the three spin current channels contributing to SMR (thermal magnon excitation, magnon capacitance, and STT, as shown in Figure 1b) exhibit anisotropy with respect to the current direction, this could be reflected in the anisotropy of the SMR ratio. This scenario is, in principle, plausible for several reasons: first, both the thermal magnon excitation [16, 49] and STT contributions [2, 16] depend on the spin mixing conductance, which is predicted to vary with crystal orientation due to crystal field effects [50]. Second, the magnon-related contributions depend on the magnon density of states, which is influenced by the magnon dispersion relation [15, 16]. The magnon density of states can exhibit anisotropy with respect to crystal momentum due to magnetocrystalline anisotropy (a relativistic effect) or due to anisotropic exchange interactions (a non-relativistic effect). Finally, the magnon capacitance contribution, which depends on the exchange interactions and the magnon lifetime [16, 51], may also exhibit anisotropy with respect to crystal momentum.

The anisotropic local crystal environment inherent to altermagnets naturally leads to magnetotransport properties that exhibit unconventional anisotropy with respect to the crystal direction [24–26, 52–55]. Also the chirality splitting of the magnon dispersion in altermagnets depends strongly on the crystal momentum direction [29, 30], driven by anisotropic exchange interactions. This dependence can result in crystal-direction-dependent magnon lifetimes and/or anisotropy in thermal magnon excitation, as the chirality splitting (or degeneracy) along specific crystal directions may facilitate or suppress magnon excitation. BCGO is a planar g-wave altermagnet [31], i.e. it exhibits four nodal planes in the (001)

plane. On the other hand, the anisotropy of the SMR ratio we observe in Figure 5b can be fitted with a  $-\cos 2\alpha - \cos 4\alpha$  dependence. This does not appear to be directly compatible with the g-wave symmetry but rather with the relativistic magnetic space group that is orthorhombic: when the magnetic moments point along  $\langle 110 \rangle$  axes, the space group is  $Cm'm2'$  while moments along  $\langle 100 \rangle$  the space group is  $P2121'2'$ . However, it is important to note that the anisotropy of the overall SMR ratio represents a superposition of the anisotropies from each spin current channel. In order to map the symmetry of the altermagnetic phase onto the symmetry of the anisotropic SMR signal, calculations on the magnon dispersion and electronic band structure of BCGO as well as symmetry analysis of each SMR contribution discussed above must be conducted in order to rigorously confirm the altermagnetic origin of the current-direction anisotropic SMR we observe and it represents an important future task.

Finally, we note that anisotropic SMR amplitude with respect to the crystal orientation of the current channel has been observed in single crystals of  $\alpha\text{-Fe}_2\text{O}_3$  [56] (another altermagnetic candidate material [17, 57, 58]), but this has been primarily discussed in terms of the Néel vector dynamics governed by the magnetocrystalline anisotropy. Further systematic experiments on the anisotropic SMR amplitude in altermagnets, such as  $\alpha\text{-Fe}_2\text{O}_3$ , as the MI layer could shed more light on whether it is a characteristic feature of AM insulator/HM heterostructures. Moreover, to disentangle the contributions of the different spin current channels to the SMR ratio, their different frequency-dependencies can be leveraged in SMR measurements beyond the DC limit into the THz range [16]. In addition to providing further information on the anisotropy of the different terms, such experiments could allow identifying whether any of the terms can explain the surprisingly large SMR ratio reported in the altermagnetic MIs (this work and Ref. [10]) compared to their ferromagnetic and antiferromagnetic counterparts.

#### IV. CONCLUSION

In this work, we showed that the heterostructure of Pt and a single crystal of the insulating altermagnetic candidate material  $\text{Ba}_2\text{CoGe}_2\text{O}_7$  exhibit a surprisingly high, current-direction anisotropic spin Hall magnetoresistance signal. We discussed the anisotropy in the context of magnetocrystalline anisotropy, magnetic domains, and variation in the electric polarization and concluded that these factors are unlikely to provide a complete explanation. Finally, we discussed the possible mechanisms through which the inherently anisotropic local crystal environment of  $\text{Ba}_2\text{CoGe}_2\text{O}_7$ , characteristic of altermagnets, could give rise to the current-direction anisotropic SMR. To unambiguously assign the anisotropic SMR amplitude to the altermagnetic phase of  $\text{Ba}_2\text{CoGe}_2\text{O}_7$ , a quantitative theoretical model that takes into account the possible altermagnetic features in all the various contributions to SMR as well as further systematic SMR studies - in particular in the THz regime - on heterostructures with a heavy metal and an altermagnetic insulator are required. Overall, our findings

represent an initial step toward a deeper understanding of altermagnetic features in spin Hall magnetoresistance.

#### ACKNOWLEDGMENTS

The work was supported by the Grant Agency of the Czech Republic Grant No. 22-17899K, the Dioscuri Program LV23025 funded by MPG and MEYS, TERA FIT - CZ.02.01.01/00/22\_008/0004594 funded by OP JAK, call Excellent Research, the Deutsche Forschungsgemeinschaft (DFG, German Research Foundation) via projects 445976410 and 490730630, via , via Project-ID No. 446571927 and the SFB 1432, Project-ID No. 425217212, and the Grant Agency of the Charles University through grants No. 166123 and SVV-2024-260720. We also gratefully acknowledge technical support and advice by the nano.lab facility of the University of Konstanz. V. K. was supported by the Alexander von Humboldt Foundation. AUBW and BB were supported by DFG through SFB 1143, project-id 247310070 and the Würzburg-Dresden Cluster of Excellence on Complexity and Topology in Quantum Matter ct.qmat (EXC 2147, project-id 390858490).

- [1] H. Nakayama, M. Althammer, Y.-T. Chen, K. Uchida, Y. Kajiwara, D. Kikuchi, T. Ohtani, S. Geprags, M. Opel, S. Takahashi, R. Gross, G. E. W. Bauer, S. T. B. Goennenwein, and E. Saitoh, Spin Hall magnetoresistance induced by a nonequilibrium proximity effect, *Phys. Rev. Lett.* **110**, 206601 (2013).
- [2] Y.-T. Chen, S. Takahashi, H. Nakayama, M. Althammer, S. T. B. Goennenwein, E. Saitoh, and G. E. W. Bauer, Theory of spin Hall magnetoresistance, *Phys. Rev. B* **87**, 144411 (2013).
- [3] M. Althammer, S. Meyer, H. Nakayama, M. Schreier, S. Altmannshofer, M. Weiler, H. Huebl, S. Geprags, M. Opel, R. Gross, D. Meier, C. Klewe, T. Kuschel, J.-M. Schmalhorst, G. Reiss, L. Shen, A. Gupta, Y.-T. Chen, G. E. W. Bauer, E. Saitoh, and S. T. B. Goennenwein, Quantitative study of the spin Hall magnetoresistance in ferromagnetic insulator/normal metal hybrids, *Phys. Rev. B* **87**, 224401 (2013).
- [4] M. Isasa, A. Bedoya-Pinto, S. Velez, F. Golmar, F. Sanchez, L. E. Hueso, J. Fontcuberta, and F. Casanova, Spin Hall magnetoresistance at Pt/CoFe<sub>2</sub>O<sub>4</sub> interfaces and texture effects, *Applied Physics Letters* **105**, 142402 (2014).
- [5] J. H. Han, C. Song, F. Li, Y. Y. Wang, Q. H. Yang, and F. Pan, Antiferromagnet-controlled spin current transport in SrMnO<sub>3</sub>/Pt hybrids, *Phys. Rev. B* **90**, 144431 (2014).
- [6] S. Putter, S. Geprags, R. Schlitz, M. Althammer, A. Erb, R. Gross, and S. T. B. Goennenwein, Impact of the interface quality of Pt/YIG(111) hybrids on their spin Hall magnetoresistance, *Applied Physics Letters* **110**, 012403 (2017).
- [7] B.-W. Dong, J. Cramer, K. Ganzhorn, H. Y. Yuan, E.-J. Guo, S. T. B. Goennenwein, and M. Klaui, Spin Hall magnetoresistance in the non-collinear ferrimagnet GdIG close to the compensation temperature, *Journal of Physics: Condensed Matter* **30**, 035802 (2017).
- [8] G. R. Hoogeboom, A. Aqeel, T. Kuschel, T. T. M. Palstra, and B. J. van Wees, Negative spin Hall magnetoresistance of Pt on the bulk easy-plane antiferromagnet NiO, *Applied Physics Letters* **111**, 052409 (2017).
- [9] J. Fischer, O. Gomonay, R. Schlitz, K. Ganzhorn, N. Vlietstra, M. Althammer, H. Huebl, M. Opel, R. Gross, S. T. B. Goennenwein, and S. Geprags, Spin Hall magnetoresistance in antiferromagnet/heavy-metal heterostructures, *Phys. Rev. B* **97**, 014417 (2018).
- [10] J. Fischer, M. Althammer, N. Vlietstra, H. Huebl, S. T. Goennenwein, R. Gross, S. Geprags, and M. Opel, Large spin Hall magnetoresistance in antiferromagnetic  $\alpha$ -Fe<sub>2</sub>O<sub>3</sub>/Pt heterostructures, *Phys. Rev. Appl.* **13**, 014019 (2020).
- [11] L. J. Cornelissen, J. Liu, R. A. Duine, J. B. Youssef, and B. J. van Wees, Long-distance transport of magnon spin information in a magnetic insulator at room temperature, *Nature Physics* **11**, 1022–1026 (2015).
- [12] S. T. B. Goennenwein, R. Schlitz, M. Pernpeintner, K. Ganzhorn, M. Althammer, R. Gross, and H. Huebl, Non-local magnetoresistance in YIG/Pt nanostructures, *Applied Physics Letters* **107**, 172405 (2015).
- [13] S. Velez, A. Bedoya-Pinto, W. Yan, L. E. Hueso, and F. Casanova, Competing effects at Pt/YIG interfaces: spin Hall magnetoresistance, magnon excitations, and magnetic frustration, *Phys. Rev. B* **94**, 174405 (2016).
- [14] X.-P. Zhang, F. S. Bergeret, and V. N. Golovach, Theory of spin Hall magnetoresistance from a microscopic perspective, *Nano Letters* **19**, 6330–6337 (2019).
- [15] T. Kato, Y. Ohnuma, and M. Matsuo, Microscopic theory of spin Hall magnetoresistance, *Phys. Rev. B* **102**, 094437 (2020).
- [16] D. A. Reiss, T. Kampfrath, and P. W. Brouwer, Theory of spin Hall magnetoresistance in the ac terahertz regime, *Phys. Rev. B* **104**, 024415 (2021).
- [17] L. Šmejkal, J. Sinova, and T. Jungwirth, Beyond conventional ferromagnetism and antiferromagnetism: A phase with nonrelativistic spin and crystal rotation symmetry, *Phys. Rev. X* **12**, 031042 (2022).
- [18] L. Šmejkal, J. Sinova, and T. Jungwirth, Emerging research landscape of altermagnetism, *Phys. Rev. X* **12**, 040501 (2022).
- [19] T. Jungwirth, R. M. Fernandes, J. Sinova, and L. Smejkal, *Altermagnets and beyond: Nodal magnetically-ordered phases* (2024), arXiv:2409.10034 [cond-mat.mtrl-sci].
- [20] T. Jungwirth, R. M. Fernandes, E. Fradkin, A. H. MacDonald, J. Sinova, and L. Smejkal, *From supefluid 3he to altermagnets* (2024), arXiv:2411.00717 [cond-mat.mtrl-sci].
- [21] L. Šmejkal, R. Gonzalez-Hernandez, T. Jungwirth, and J. Sinova, Crystal time-reversal symmetry breaking and spontaneous hall effect in collinear antiferromagnets, *Science Advances* **6**, 10.1126/sciadv.aaz8809 (2020).
- [22] I. I. Mazin, K. Koepernik, M. D. Johannes, R. Gonzalez-Hernandez, and L. Šmejkal, Prediction of unconventional magnetism in doped fesb<sub>2</sub>, *Proceedings of the National Academy of Sciences* **118**, 10.1073/pnas.2108924118 (2021).
- [23] R. Gonzalez-Hernandez, L. Šmejkal, K. Vyborny, Y. Yahagi, J. Sinova, T. Jungwirth, and J. Železny, Efficient electrical spin splitter based on nonrelativistic collinear antiferromagnetism, *Phys. Rev. Lett.* **126**, 127701 (2021).
- [24] A. Bose, N. J. Schreiber, R. Jain, D.-F. Shao, H. P. Nair, J. Sun, X. S. Zhang, D. A. Muller, E. Y. Tsymbal, D. G. Schlom, and D. C. Ralph, Tilted spin current generated by the collinear antiferromagnet ruthenium dioxide, *Nature Electronics* **5**, 267–274 (2022).
- [25] S. Karube, T. Tanaka, D. Sugawara, N. Kadoguchi, M. Kohda, and J. Nitta, Observation of spin-splitter torque in collinear antiferromagnetic RuO<sub>2</sub>, *Phys. Rev. Lett.* **129**, 137201 (2022).
- [26] H. Bai, Y. C. Zhang, Y. J. Zhou, P. Chen, C. H. Wan, L. Han, W. X. Zhu, S. X. Liang, Y. C. Su, X. F. Han, F. Pan, and C. Song, Efficient spin-to-charge conversion via altermagnetic spin splitting effect in antiferromagnet RuO<sub>2</sub>, *Phys. Rev. Lett.* **130**, 216701 (2023).
- [27] L. Šmejkal, A. B. Hellenes, R. Gonzalez-Hernandez, J. Sinova, and T. Jungwirth, Giant and tunneling magnetoresistance in unconventional collinear antiferromagnets with nonrelativistic spin-momentum coupling, *Phys. Rev. X* **12**, 011028 (2022).
- [28] K. Samanta, Y.-Y. Jiang, T. R. Paudel, D.-F. Shao, and E. Y. Tsymbal, Tunneling magnetoresistance in magnetic tunnel junctions with a single ferromagnetic electrode, *Phys. Rev. B* **109**, 174407 (2024).
- [29] L. Šmejkal, A. Marmodoro, K.-H. Ahn, R. Gonzalez-Hernandez, I. Turek, S. Mankovsky, H. Ebert, S. W. D’Souza, O. Šipr, J. Sinova, and T. Jungwirth, Chiral magnons in altermagnetic RuO<sub>2</sub>, *Phys. Rev. Lett.* **131**, 256703 (2023).
- [30] Q. Cui, B. Zeng, P. Cui, T. Yu, and H. Yang, Efficient spin Seebeck and spin Nernst effects of magnons in altermagnets, *Phys. Rev. B* **108**, L180401 (2023).
- [31] L. Šmejkal, *Altermagnetic multiferroics and altermagnetoelectric effect* (2024), arXiv:2411.19928 [cond-mat.mtrl-sci].
- [32] V. Hutanu, A. Sazonov, H. Murakawa, Y. Tokura, B. Nafradi, and D. Chernyshov, Symmetry and structure of multiferroic Ba<sub>2</sub>CoGe<sub>2</sub>O<sub>7</sub>, *Phys. Rev. B* **84**, 212101 (2011).

- [33] V. Hutanu, A. Sazonov, M. Meven, H. Murakawa, Y. Tokura, S. Bordács, I. Kézsmárki, and B. Náfrádi, Determination of the magnetic order and the crystal symmetry in the multiferroic ground state of  $\text{Ba}_2\text{CoGe}_2\text{O}_7$ , *Phys. Rev. B* **86**, 104401 (2012).
- [34] T. Sato, Magnetic property of  $\text{Ba}_2\text{CoGe}_2\text{O}_7$ , *Physica B: Condensed Matter* **329–333**, 880–881 (2003).
- [35] H. T. Yi, Y. J. Choi, S. Lee, and S.-W. Cheong, Multiferroicity in the square-lattice antiferromagnet of  $\text{Ba}_2\text{CoGe}_2\text{O}_7$ , *Applied Physics Letters* **92**, 212904 (2008).
- [36] I. V. Solovyev, Magnetization-induced local electric dipoles and multiferroic properties of  $\text{Ba}_2\text{CoGe}_2\text{O}_7$ , *Phys. Rev. B* **91**, 224423 (2015).
- [37] H. Thoma, V. Hutanu, R. Dutta, A. Gukasov, V. Kocsis, Y. Tokunaga, Y. Taguchi, Y. Tokura, I. Kézsmárki, G. Roth, and M. Angst, Magnetic order and sign of the Dzyaloshinskii–Moriya interaction in 2-D antiferromagnet  $\text{Ba}_2\text{CoGe}_2\text{O}_7$  under applied magnetic field, *IEEE Transactions on Magnetics* **58**, 1–5 (2022).
- [38] H. Murakawa, Y. Onose, S. Miyahara, N. Furukawa, and Y. Tokura, Ferroelectricity induced by spin-dependent metal-ligand hybridization in  $\text{Ba}_2\text{CoGe}_2\text{O}_7$ , *Phys. Rev. Lett.* **105**, 137202 (2010).
- [39] J. Vít, J. Viírok, L. Peedu, T. Rõõm, U. Nagel, V. Kocsis, Y. Tokunaga, Y. Taguchi, Y. Tokura, I. Kézsmárki, P. Balla, K. Penc, J. Romhányi, and S. Bordács, In situ electric-field control of THz nonreciprocal directional dichroism in the multiferroic  $\text{Ba}_2\text{CoGe}_2\text{O}_7$ , *Phys. Rev. Lett.* **127**, 157201 (2021).
- [40] V. Hutanu, A. P. Sazonov, M. Meven, G. Roth, A. Gukasov, H. Murakawa, Y. Tokura, D. Szaller, S. Bordács, I. Kézsmárki, V. K. Guduru, L. C. J. M. Peters, U. Zeitler, J. Romhányi, and B. Náfrádi, Evolution of two-dimensional antiferromagnetism with temperature and magnetic field in multiferroic  $\text{Ba}_2\text{CoGe}_2\text{O}_7$ , *Phys. Rev. B* **89**, 064403 (2014).
- [41] R. Schlitz, T. Kosub, A. Thomas, S. Fabretti, K. Nielsch, D. Makarov, and S. T. B. Goennenwein, Evolution of the spin Hall magnetoresistance in  $\text{Cr}_2\text{O}_3/\text{Pt}$  bilayers close to the Néel temperature, *Applied Physics Letters* **112**, 132401 (2018).
- [42] M. Lammel, R. Schlitz, K. Geisendorff, D. Makarov, T. Kosub, S. Fabretti, H. Reichlova, R. Huebner, K. Nielsch, A. Thomas, and S. T. B. Goennenwein, Spin Hall magnetoresistance in heterostructures consisting of noncrystalline paramagnetic YIG and Pt, *Applied Physics Letters* **114**, 252402 (2019).
- [43] K. Oyanagi, J. M. Gomez-Perez, X.-P. Zhang, T. Kikkawa, Y. Chen, E. Sagasta, A. Chuvilin, L. E. Hueso, V. N. Golovach, F. S. Bergeret, F. Casanova, and E. Saitoh, Paramagnetic spin Hall magnetoresistance, *Phys. Rev. B* **104**, 134428 (2021).
- [44] C. Burrowes, B. Heinrich, B. Kardasz, E. A. Montoya, E. Girt, Y. Sun, Y.-Y. Song, and M. Wu, Enhanced spin pumping at yttrium iron garnet/Au interfaces, *Applied Physics Letters* **100**, 092403 (2012).
- [45] M. B. Jungfleisch, V. Lauer, R. Neb, A. V. Chumak, and B. Hillebrands, Improvement of the yttrium iron garnet/platinum interface for spin pumping-based applications, *Applied Physics Letters* **103**, 022411 (2013).
- [46] Z. Qiu, K. Ando, K. Uchida, Y. Kajiwara, R. Takahashi, H. Nakayama, T. An, Y. Fujikawa, and E. Saitoh, Spin mixing conductance at a well-controlled platinum/yttrium iron garnet interface, *Applied Physics Letters* **103**, 092404 (2013).
- [47] Z. Qiu, D. Hou, K. Uchida, and E. Saitoh, Influence of interface condition on spin-Seebeck effects, *Journal of Physics D: Applied Physics* **48**, 164013 (2015).
- [48] Y. Wu, Z. Xu, J. Chen, X. Xu, J. Miao, and Y. Jiang, The anisotropy of spin Hall magnetoresistance in Pt/YIG structures, *Applied Physics A* **127**, 419 (2021).
- [49] L. J. Cornelissen, K. J. H. Peters, G. E. W. Bauer, R. A. Duine, and B. J. van Wees, Magnon spin transport driven by the magnon chemical potential in a magnetic insulator, *Phys. Rev. B* **94**, 014412 (2016).
- [50] A. B. Cahaya, A. O. Leon, and G. E. W. Bauer, Crystal field effects on spin pumping, *Phys. Rev. B* **96**, 144434 (2017).
- [51] O. Franke, D. Akrap, U. Gems, D. A. Reiss, and P. W. Brouwer, *Theory of ac magnetoelectric transport in normal-metal – magnetic-insulator heterostructures* (2024), arXiv:2408.13099 [cond-mat.mes-hall].
- [52] Z. Feng, X. Zhou, L. Šmejkal, L. Wu, Z. Zhu, H. Guo, R. González-Hernández, X. Wang, H. Yan, P. Qin, X. Zhang, H. Wu, H. Chen, Z. Meng, L. Liu, Z. Xia, J. Sinova, T. Jungwirth, and Z. Liu, An anomalous hall effect in altermagnetic ruthenium dioxide, *Nature Electronics* **5**, 735–743 (2022).
- [53] H. Bai, L. Han, X. Y. Feng, Y. J. Zhou, R. X. Su, Q. Wang, L. Y. Liao, W. X. Zhu, X. Z. Chen, F. Pan, X. L. Fan, and C. Song, Observation of spin splitting torque in a collinear antiferromagnet  $\text{ruo}_2$ , *Phys. Rev. Lett.* **128**, 197202 (2022).
- [54] R. D. Gonzalez Betancourt, J. Zubáč, K. Geisendorff, P. Ritzinger, B. Růžicková, T. Kotte, J. Železný, K. Olejník, G. Springholz, B. Büchner, A. Thomas, K. Výborný, T. Jungwirth, H. Reichlová, and D. Kriegner, Anisotropic magnetoresistance in altermagnetic mnte, npj Spintronics **2**, 10.1038/s44306-024-00046-z (2024).
- [55] M. Leiviskä, J. Rial, A. Bad'ura, R. L. Seeger, I. Kounta, S. Beckert, D. Kriegner, I. Joumard, E. Schmoranzzerová, J. Sinova, O. Gomonay, A. Thomas, S. T. B. Goennenwein, H. Reichlová, L. Šmejkal, L. Michez, T. c. v. Jungwirth, and V. Baltz, Anisotropy of the anomalous hall effect in thin films of the altermagnet candidate  $\text{mn}_5\text{si}_3$ , *Phys. Rev. B* **109**, 224430 (2024).
- [56] R. Lebrun, A. Ross, O. Gomonay, S. A. Bender, L. Baldrati, F. Kronast, A. Qaiumzadeh, J. Sinova, A. Brataas, R. A. Duine, and M. Kläui, Anisotropies and magnetic phase transitions in insulating antiferromagnets determined by a spin-Hall magnetoresistance probe, *Communications Physics* **2**, 50 (2019).
- [57] X. H. Verbeek, D. Voderholzer, S. Schären, Y. Gachnang, N. A. Spaldin, and S. Bhowal, *Non-relativistic ferromagnetotriakontadipolar order and spin splitting in hematite* (2024), arXiv:2405.10675 [cond-mat.str-el].
- [58] E. F. Galindez-Ruales, L. Šmejkal, S. Das, E. Baek, C. Schmitt, F. Fuhrmann, A. Ross, R. González-Hernández, A. Rothschild, J. Sinova, C. Y. You, G. Jakob, and M. Kläui, *Altermagnetism in the hopping regime* (2024), arXiv:2310.16907 [cond-mat.mtrl-sci].